Optics Letters

Estimation of atmospheric refractive index structure constant using an InGaAs/InP single-photon detector

Pu Jiang,[1] Haiyun Xia,[1,2,3,*] Jiadong Hu,[2] and Tianwen Wei[2]

[1]School of Earth and Space Science, University of Science and Technology of China, Hefei 230026, China
[2]School of atmospheric physics, Nanjing University of Information Science and Technology, Nanjing 210044, China
[3]Hefei National Laboratory for Physical Sciences at the Microscale, USTC, Hefei 230026, China
*hsia@ustc.edu.cn

Received 12 September 2023; revised 24 October 2023; accepted 26 October 2023; posted 26 October 2023; published 18 November 2023

Remote sensing of atmospheric refractive index structure constant (C_n^2) using lidar incorporating a single-photon detector (SPD) is proposed. The influence of turbulence on the fiber coupling efficiency with different fiber modes is analyzed. C_n^2 can be derived from the ratio of the backscattering signals counted on single-mode and multimode fiber-coupling channels of the SPD. In the experiment, by eliminating the shot noise effect on the fluctuation of the ratio, the lowest coupling ratio is used to retrieve C_n^2 and demonstrated by comparing to the results measured from a large aperture scintillometer (LAS). Good agreement between results from the LAS and the lidar is achieved. The correlation coefficients are 0.90, 0.89, and 0.89, under three different weather conditions.

https://doi.org/10.1364/OL.505631

Atmospheric turbulence plays a vital role in the areas of astronomy [1], free-space optical communication [2], and wind field retrieval [3]. Turbulence brings the optical angle-of-arrival fluctuation, laser beam wander, and scintillation [4]. Then it affects the coherence of the emitted laser beam and reduces the system detection efficiency. The refractive index structure constant C_n^2 is a parameter that directly represents the fluctuation intensity of the spatial refractive index.

At present, there are some common methods for C_n^2 estimation. Combining with meteorological data, C_n^2 can be measured through the temperature structure constant C_T^2 [5,6] or through the turbulent kinetic energy dissipation rate (TKEDR) [7]. The method using the TKEDR needs multiple atmospheric parameters and complex algorithm. According to the intensity scintillation principle, the large aperture scintillometer (LAS) can measure the path-averaged C_n^2 within a chosen distance [8]. The LAS can estimate C_n^2 directly, but the transmitter and the receiver installed at a certain distance need to be aligned in the optical axis and calibrated periodically, restraining its application scenarios, especially in the direction of detection. In this work, a concise and compact single-photon lidar for turbulence estimation is demonstrated, where the turbulence effect on coupling efficiency from telescope to single-mode fiber (SMF) or multimode fiber (MMF) is analyzed.

The lidar system is shown on the left of Fig. 1. The seeder emits a continuous wave (CW) at 1548.5 nm; then the CW is chopped and frequency-shifted at 80 MHz by an acousto-optic modulator (AOM). After that, the laser is amplified by using an erbium-doped fiber amplifier (EDFA) and pointed to the atmosphere through a double "D" shaped telescope. At the receiving end, an iris is placed in front of the coupler to ensure the SMF and MMF ends share the same area of the receiving lens. Then, the backscattering signal divided by a 3-dB beam splitter (BS) and then coupled onto the ends of SMF and MMF. Two inline narrow bandpass interferometer filters at 1548.5 nm with bandwidth of 0.1 nm are used to suppress the background noise. Finally, the signals are detected by a dual-channel single-photon detector (SPD). There are three main types of SPDs: superconducting nanowire single-photon detector [9], upconversion single-photon detector [10], and InGaAs/InP SPD [11]. The InGaAs/InP SPD is adopted considering its advantages of small size and polarization-independent. Some key parameters of the lidar system are listed in Table 1.

After the iris, the effective diameter of the coupler is D_e with a focal length of f_r. The fiber-mode field radiuses of the SMF and MMF are W_s and W_m, respectively, while the fiber coupling efficiency is easily affected by the atmospheric turbulence. As depicted in the right of Fig. 1, a random space optical field E_i represents the influence of turbulence upon the laser phase distribution. E_i is simulated by a phase screen [12] (the color bar indicates the phase shift).

On the one hand, the fiber coupling efficiency of SMF, η_s, is defined as the ratio of the average power coupled into the receiving fiber, to the average power in the aperture plane of the coupler. After normalizing the radial integration variables r_1 and r_2 to the coupler lens radius ($x_1 = 2r_1/D_e$ and $x_2 = 2r_2/D_e$), η_s can be given by a double integral as the following [13]:

$$\eta_s = 8a^2 \int_0^1 \int_0^1 \exp\left[-(a^2 + \frac{A_R}{A_C})({x_1}^2 + {x_2}^2)\right] \times I_0(2\frac{A_R}{A_C}x_1x_2)x_1x_2dx_1dx_2, \quad (1)$$

where a is the ratio of the coupling lens radius to the radius of the backpropagated fiber mode, $a = D_e\pi W_s/2\lambda f_r$ and λ is the wavelength. $A_R = \pi D_e^2/4$ is the area of the receiving aperture, $A_C = \pi\rho_e^2$ stands for the spatial coherence area, also called as speckle size. ρ_e is the effective field coherence length, and $\rho_e = [1/\rho_0^2 + (\pi\omega_t/\lambda R)^2]^{-1/2}$ [14]. The first term is the field coherence caused by the turbulence, where $\rho_0 = (1.46C_n^2k^2R)^{-3/5}$, $k = 2\pi/\lambda$ is the wave number, and R is the transmission distance. The

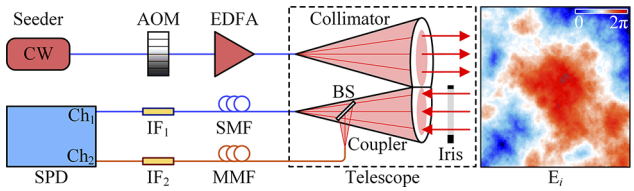

Fig. 1. Optical layout of the lidar system. AOM, acousto-optic modulator; EDFA, erbium-doped fiber amplifier; BS, beam splitter; SMF, single-mode fiber; MMF, multimode fiber; IF, interferometer filter; SPD, single-photon detector. Schematic diagram of the turbulent incident radiation E_i.

Table 1. Key Parameters of the Turbulence Lidar

Parameter	Value
Laser	
Wavelength (λ)	1548.5 nm
Pulse width (τ_P)	200 ns
Pulse energy (E_P)	110 μJ
Repetition frequency (ν)	10 kHz
Collimator	
Lens' diameter (D_t)	95.5 mm
Focal length (f_t)	500 mm
Lens' diameter (D_r)	70.5 mm
Coupler	
Lens' effective diameter (D_e)	45 mm
Focal length (f_r)	210 mm
Divergence angle (ϕ)	0.214
SMF	
Mode field diameter ($2W_s$)	9 μm
Numerical aperture (NA_s)	0.12
MMF	
Mode field diameter ($2W_m$)	50 μm
Numerical aperture (NA_m)	0.22

second term is caused by the spatially incoherent source, which can be described by the van CittertZernike theorem [15]. ω_t is the average radius of the normalized irradiance in the target plane, $\omega_t^2 = \omega_0^2[(1 - R/r_f)^2 + (R/R_r)^2] + (\lambda R/\pi\rho_0)^2$, where ω_0 is the $1/e^2$ intensity radius of the collimator lens, r_f is the radius of the phase curvature (r_f is 1 km in our lidar system), and $R_r = \pi\omega_0^2/\lambda$ is the Rayleigh length. $I_0(\,)$ means the modified Bessel function of the first kind and zero order.

For a given optical transmitting and receiving system that is listed in Table 1, a can be calculated as 0.98. Therefore, the behavior of η_s only depends on A_R/A_C, which is related to C_n^2 and R. Then, the numerical results of η_s are estimated as shown in Fig. 2(a)(b). One can find that η_s declines monotonously as the growing C_n^2.

On the other hand, the beam propagation factor (M^2 factor) that describes the quality of the laser beam propagating through the atmosphere is used to estimate the coupling efficiency into a multimode fiber (η_m), which can be expressed as [16]

$$\eta_m = \eta_{re}\left[1 - \exp(-\frac{2M_F^2}{M^2})\right]^2, \tag{2}$$

where η_{re} is the reflection loss originating from the input and output surfaces, $\eta_{re} = (1 - r_1) \times (1 - r_2)$. r_1 and r_2 mean the directions from air to silica and silica to air. They are both 0.034 when the refractive indexes of silica and air are 1.45

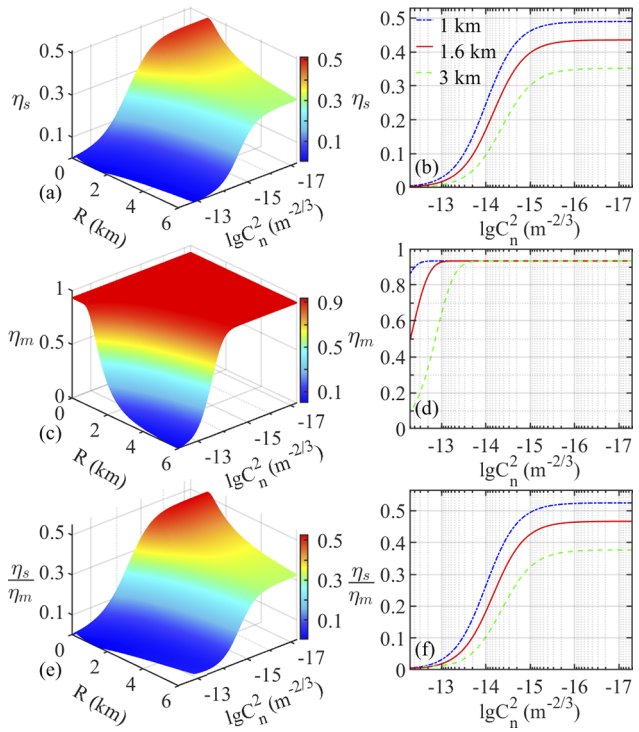

Fig. 2. Numerical results of (a), (b) η_s, (c), (d) η_m, and (e), (f) η_s/η_m with different C_n^2 and R.

and 1, respectively. M_F^2 can be expressed as: $M_F^2 = \pi W_m\theta/\lambda$ ($\sin\theta = \mathrm{NA}_m$). M^2 can be estimated by [17]

$$M^2 = \left[(M_0^2)^2 + 2\omega_0^2k^2TR + \frac{8}{3\omega_0^2}TR^3 + \frac{4}{3}k^2T^2R^4\right]^{1/2}, \tag{3}$$

where $M_0^2 = \pi\omega\phi/\lambda$, ω is the laser beam radius and ϕ is divergence angle before coupling into a fiber. ω_0 is the beam waist of the transmitting laser and $T = 7.6113C_n^2$.

According to the parameters listed in Table 1, η_m can be depicted in Fig. 2(c)(d). Compared with η_s, η_m has the similar feature of monotonously decreasing with the growing C_n^2. But, η_m shows low sensitivity to turbulence.

In practice, the overall average power in the aperture plane of the telescope is hard to be precisely measured due to the limited size of the active diameter of the photodetector. Therefore, it is difficult to directly estimate the η_s and η_m, separately.

In this work, as shown in Fig. 1, the photon number counted on the SMF-coupled channel N_s or the MMF-coupled channel N_m can be expressed according to the lidar equation as follows [10]:

$$N_i(R) = \frac{E}{h\upsilon}\frac{c\tau}{2}A\eta_i\eta_{qi}\frac{O(R)}{R^2}\beta(R)T_r(R), \tag{4}$$

where the subscript i indicates s (SMF) or m (MMF). $N_i(R)$ is the photon number at a distance of R. E is the laser pulse energy, h is the Planck constant, and υ is the optical frequency. c is the speed of light, and τ is the pulse duration of the laser. A is the area of the coupler. η_i is the fiber coupling efficiency, and η_{qi} is the quantum efficiency. $O(R)$ is the geometrical overlap factor. $\beta(R)$ is the Mie volume backscattering coefficients, and $T_r(R)$ is the round trip atmosphere transmission.

From Eq. (4), one can find that the difference between N_s and N_m are introduced by η_i and η_{qi}. All the other parameters are the

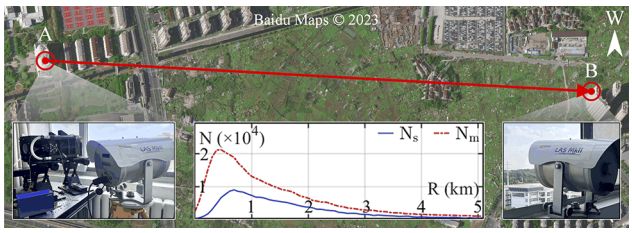

Fig. 3. Instruments installation labeled in the map. Inset is the raw photon numbers counted on two channels accumulated over 100 s.

same since the backscattering signals detected in two channels travel through the same atmosphere path and share the same optics. Therefore, the ratio of them ($\eta(R)$) can be expressed as

$$\eta(R) = \frac{N_s(R)}{N_m(R)} = \frac{\eta_{qs}\eta_s(C_n^2, R)}{\eta_{qm}\eta_m(C_n^2, R)}. \tag{5}$$

Similar to the optical efficiency of the telescope, η_{qi} can be calibrated in the system initialization and treated as a constant. It should be noted that the numerical results of $\eta_s(C_n^2, R)$ and $\eta_m(C_n^2, R)$ in Fig. 2 have not considered the fluctuations of coupling efficiencies over time. So, in practice, Eq. (5) can only be used after suitable data processing. Then, C_n^2 at a given transmission distance R can be retrieved according to the recorded $N_s(R)$ and $N_m(R)$.

A verification experiment was carried out at the campus of the Nanjing University of Information Science and Technology (NUIST, 32°12′22″N, 118°42′17″E) from April to May, 2023. The lidar system is installed on the 9th floor (altitude of 30 m) of a building, pointing out in the north direction as shown in Fig. 3 from site A. For easy comparison, the transmitting end of the LAS (Kipp & Zonen, LAS MKII) is set up near the lidar, and the receiving end is placed at the same altitude of another building at 1.6 kilometers away (site B). The outgoing laser beam of the lidar is adjusted parallel to the LAS to make sure they are detecting the same atmosphere path. The raw resolutions of N_s and N_m are set as 1 s and 60 m, respectively. As an example, the accumulated signals N_s and N_m over 100 s at 05:00, 27 April, 2023, are shown as the inset in the middle of Fig. 3.

The experiment results under three different weather conditions are analyzed. The raw data and averaged photon numbers, η at the range of 1.6 km are shown in Fig. 4(a)(b). Due to the aerosol hygroscopic growth, one can see that N_s and N_m vary greatly as the relative humidity in Fig. 4(d) and the atmospheric temperature in Fig. 4(f) changes. The atmospheric visibility in Fig. 4(e) shows a negative correlation with the relative humidity. The results of η in Fig. 4(b) show rapid fluctuations along the time, which proves the previous notice about using Eq. (5). Obviously, the amplitude of this fluctuation shows a positive correlation with the C_n^2 measured by the LAS as depicted in Fig. 4(c).

From Eq. (5), there is $\delta_\eta^2 = \delta_s^2 + \delta_m^2$, where δ_η, δ_s, and δ_m means the relative error of η, N_s, and N_m. $\delta_\eta = \sigma_\eta/\bar{\eta}$, respectively, where σ_η is the 1σ standard deviation of the fluctuations of η.

In theory, the fast fluctuations of N_s and N_m are due to the combined effect of shot noise in photon counting scheme and turbulence, which yields $\delta_s^2 = \delta_{sp}^2 + \delta_{st}^2$ and $\delta_m^2 = \delta_{mp}^2 + \delta_{mt}^2$. Where δ_{sp} and δ_{mp} mean the relative errors due to shot noise, δ_{st} and δ_{mt} mean the relative errors due to turbulence. So, δ_η^2 can be separated into two parts according to the effect of shot noise $\delta_p^2 = \delta_{sp}^2 + \delta_{mp}^2$ and turbulence $\delta_t^2 = \delta_{st}^2 + \delta_{mt}^2$.

Assume the shot noise of the SPD follows a Poisson random process [18], δ_{sp} and δ_{mp} can be estimated by $\bar{N}_s^{-1/2}$ and $\bar{N}_m^{-1/2}$. So, δ_t^2 can be calculated as

$$\delta_t^2 = \delta_\eta^2 - (\overline{N_s}^{-1} + \overline{N_m}^{-1}). \tag{6}$$

Then, the fluctuations of η resulting from shot noise $\sigma_p = \delta_p \times \bar{\eta}$ and turbulence $\sigma_t = \delta_t \times \bar{\eta}$ can be obtained. The results of $\bar{\eta} \pm \sigma_p$ and $\bar{\eta} \pm \sigma_t$ are shown as yellow and blue areas in Fig. 4(b).

Based on σ_t, the $\bar{\eta} \pm 3\sigma_t$ lines are also drawn in Fig. 4(b), which represent the highest and lowest fiber coupling efficiency

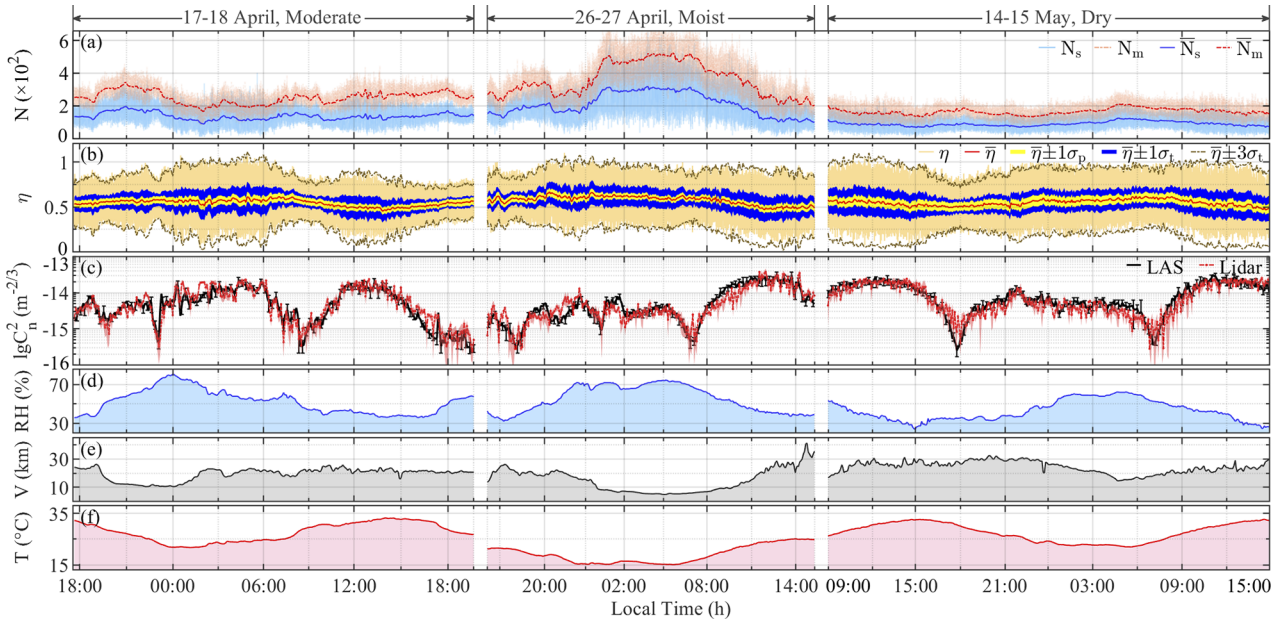

Fig. 4. Experiment results under three different weather conditions. (a) Raw data and averaged photon numbers at the distance of 1.6 km. (b) Raw data and averaged η, 1σ standard deviation of the fluctuations of η resulting from shot noise σ_p and turbulence σ_t. (c) C_n^2 results estimated by LAS and lidar, (d) relative humidity, (e) atmospheric visibility, and (f) temperature.

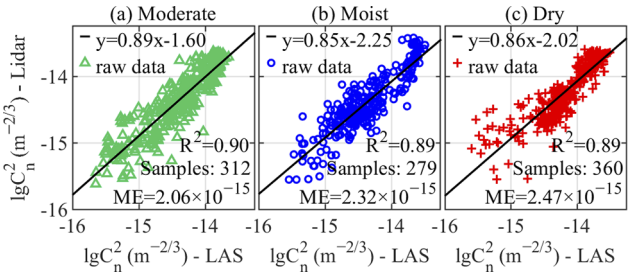

Fig. 5. C_n^2 comparison results from LAS and lidar under (a) moderate, (b) moist, and (c) dry weather conditions.

caused by turbulence. Considering the negative correlation between η and C_n^2 revealed in Fig. 2, the lower envelope $(\bar{\eta} - 3\sigma_t)$ is used as η in Eq. (5) for C_n^2 retrieval. Besides, the η_{qs}/η_{qm} term can be calibrated before the influence of turbulence is considered according to the red line in Fig. 2(f) (η_s/η_m should be 0.46 when $C_n^2 = 10^{-16}\ m^{-2/3}$). Finally, the C_n^2 results retrieved from lidar are shown in Fig. 4(c). Both the black error bar and the pinkish-shaded area are $\pm 1\sigma$ standard deviations.

From the results, one can see that the C_n^2 measured by the two instruments matches quite well under different weather conditions. They both vary in the range between 2×10^{-16} and $3 \times 10^{-14}\ m^{-2/3}$. It proves that the strengths of the backscattering signals will not affect the behavior of this method as described in Eq. (5). The new method has high standard deviation under low signal-to-noise ratio (SNR) or C_n^2. This can be explained through the red line in Fig. 2(f). When C_n^2 is smaller than $10^{-16}\ m^{-2/3}$ or higher than $10^{-13}\ m^{-2/3}$, the slope of the line is close to zero. So, the same level of noise in the measured η can bring more fluctuation to the retrieved C_n^2 result.

The statistical analyses of the results observed under moderate, moist, and dry weather conditions are shown in Fig. 5. From the comparison results, the correlation coefficients (R^2) between the LAS and lidar in the three cases are 0.90, 0.89, and 0.89. The mean errors (ME) between them are 2.06×10^{-15}, 2.32×10^{-15}, and $2.47 \times 10^{-15}\ \mathrm{m}^{-2/3}$. The root mean square errors (RMSE) between them are 2.40×10^{-15}, 3.07×10^{-15}, and $2.17 \times 10^{-15}\ \mathrm{m}^{-2/3}$. The black lines are the linear fit of them and their slopes are 0.89, 0.85, and 0.86.

In conclusion, we proposed a new method to estimate C_n^2 based on the impact of atmospheric turbulence on the fiber coupling efficiency. Although the theory has not considered the fluctuations over time, we extracted the useful information from the original results after subtracting the effects from shot noise. The comparison results with LAS also show great consistency under three different weather conditions. The compact turbulence lidar is more flexible in the selection of experimental sites and detection direction compared to LAS. According to Eq. (5), the horizontal and vertical C_n^2 profile with distance resolution can be retrieved theoretically if the SNR is high enough. To achieve this, a laser with higher pulse energy and an SPD with higher quantum efficiency are needed in the future.

Funding. National Ten Thousand Talent Program in China; Strategic Priority Research Program of Chinese Academy of Sciences (XDA22040601).

Acknowledgments. The authors thank Prof. Renmin Yuan, Dr. Manyi Li, Dr. Yunpeng Zhang, Dr. Lu Wang, and Dr. Dawei Tang for their help with the paper writing and experiments.

Disclosures. The authors declare no conflicts of interest.

Data availability. Data underlying the results presented in this paper are not publicly available at this time but may be obtained from the authors upon reasonable request.

REFERENCES

1. L. Deng, F. Yang, X. Chen, *et al.*, Nature **596**, 353 (2021).
2. Y. Ren, H. Huang, G. Xie, *et al.*, Opt. Lett. **38**, 4062 (2013).
3. J. Yuan, H. Xia, T. Wei, *et al.*, Opt. Express **28**, 37406 (2020).
4. J. Libich, J. Perez, S. Zvanovec, *et al.*, Appl. Opt. **56**, 336 (2017).
5. M. van Iersel, D. A. Paulson, C. Wu, *et al.*, Appl. Opt. **58**, 6934 (2019).
6. S. L. Odintsov, V. A. Gladkikh, A. P. Kamardin, *et al.*, Atmosphere **10**, 711 (2019).
7. P. Jiang, J. Yuan, K. Wu, *et al.*, Remote Sens. **14**, 2951 (2022).
8. W. Ting-i, G. R. Ochs, and S. F. Clifford, J. Opt. Soc. Am. **68**, 334 (1978).
9. J. Qiu, H. Xia, M. Shangguan, *et al.*, Opt. Lett. **42**, 4454 (2017).
10. H. Xia, G. Shentu, M. Shangguan, *et al.*, Opt. Lett. **40**, 1579 (2015).
11. C. Yu, J. Qiu, H. Xia, *et al.*, Rev. Sci. Instrum. **89**, 103106 (2018).
12. I. Toselli, O. Korotkova, X. Xiao, *et al.*, Appl. Opt. **54**, 4740 (2015).
13. Y. Dikmelik and F. M. Davidson, Appl. Opt. **44**, 4946 (2005).
14. R. G. Frehlich and M. J. Kavaya, Appl. Opt. **30**, 5325 (1991).
15. M. Born and E. Wolf, *Principles of Optics: 60th Anniversary Edition*, 7 ed. (Cambridge University Press, 2019).
16. J. Niu and J. Xu, Opt. Commun. **274**, 315 (2007).
17. S. Arisa, Y. Takayama, H. Endo, *et al.*, Proc. SPIE **10563**, 105630Y (2014).
18. J. R. Barry and E. A. Lee, Proc. IEEE **78**, 1369 (1990).